**ORIGINAL PAPER**

# Maximum Northern Hemisphere warming rates before and after 1880 during the Common Era

Knut Lehre Seip[1,2] · Hui Wang[3]

## Abstract

We find that maximal decadal Northern Hemisphere warming increases as rapidly before as after the industrial revolution (0.86 °C decade$^{-1}$ before 1880 and 0.60–0.68 °C decade$^{-1}$ after 1880). However, whereas the number of decadal periods with large increase and decrease rates were about equal before 1880 (267 vs. 273), after 1880 there are more periods with high increase rates (35) than with high decrease rates (9). The same patterns hold for bi-decadal rates. However, for time windows greater than about 20 years, the slope in global warming with time becomes greater after 1880. After 1971, there is only one short 11 year period with negative slopes. This reflects the higher frequency of positive slopes during the industrial period caused by the contribution of greenhouse gases (GHG). Maximum temperature changes for detrended series were associated with the beginning and end of extreme warm or cold sub periods. They occurred throughout all of the Common Era. Because the detrended temperature series showed sign of a pacemaker mechanism (regular cycle periods) we suggest that ocean variabilities were a dominating mechanism for multidecadal temperature variability during the Common Era.

## 1 Introduction

It is argued in scientific journal articles, e.g., Wuebbles et al. (2017) and Neukom et al. (2019b), and in the popular press, Graver and Stenseth (2020), that the recent trend in global warming (e.g., after the industrial revolution had manifested itself around 1880) is faster than in any previous period. We here estimate how rapidly the temperature anomaly in the Northern Hemisphere (NHTA) has changed during the period 1 to 1880 and compare it to the changes in NHTA from 1881 to 2019.

Several studies address temperature variations during the Common Era, either for the whole period, e.g., Thompson et al. (2022), Christiansen and Ljungqvist (2017), and Neukom et al. (2019b), or the studies focus on particular subperiods, e.g., recently, Shi et al. (2022) on the Roman period, Wang et al. (2022) on the Medieval and Little Ice Age periods, Stoffel et al. (2022) on the Little Ice Age and the volcanic eruption cluster during that time, and Cheng et al. (2015) on the industrial period. In the result section, we will embed our results on the persistent increase or decrease in NHTA over 11 years (decadal), 21 years (bi-decadal), and 51 years periods in a wider context. We suggest three hypotheses. The first, **H1**, is that on a decadal scale, there will be steeper changes in the NHTA before the consolidation of the industrial revolution, 1880, than during the industrial (IND) era. The rationale is that large volcanic eruptions may affect NHTA dramatically. The second, **H2**, is that the steepest changes will occur just before or just after the Little Ice Age. The third, **H3**, is that we will identify the cause for the steep changes by comparing the timing of the maximum slopes with narrow temperature windows in studies where the authors also provide explanations for why certain temperature events have occurred.

In the rest of the manuscript, Section 2 describes the data sets used, and Section 3 describes the methods used. Section 4 shows the results and Section 5 discusses the results. Section 6 concludes.

✉ Knut Lehre Seip
knut.lehre.seip@oslomet.no

Hui Wang
hui.wang@noaa.gov

1   OsloMet - Oslo Metropolitan University, Pilestredet 35, N-0130 Oslo, Norway

2   Technology, Arts and Design, Oslo Metropolitan University, Postbox 4, St. Olavs Plass 0130 Oslo, Oslo, Norway

3   NOAA/NWS/NCEP/Climate Prediction Center, 5830 University Research Court, NCWCP, College Park, MD 20740, USA

## 2 Materials

We use the annual time series of the average NHTA developed by Moberg et al. ([2005](#)) from year 1 to 1979. Their calculation method is composite plus scaling (CPS), and their centennial scale amplitude is 0.56 °C. We use global temperature anomaly (GTA) data for the period 1881 to 2019 from https://data.giss.nasa.gov/gistemp/tabledata_v4/GLB.Ts.txt and we calibrated the last part of the extended Moberg data series by comparing the average values for the period 1880 to 1979 for both series. The average values were −0.158 (Moberg) and −0.154 (NASA) data respectively. The Moberg data correlates highly with 13 other reconstructions of the NHTA during the last 1000 to 2000 years (Christiansen and Ljungqvist [2017](#)). Warm anomalies occurred around the years 1320, 1420, 1560, and 1780. Cold anomalies occurred around the years 1260, 1450, and 1820.

A recent reconstruction of GTA was completed by PAGE2k ([2017](#)). The authors develop five series, and we compare their GTA series that are based on the median value of the underlying series to NHTA. The series were obtained from https://www.ncbi.nlm.nih.gov/pmc/articles/PMC6675609/.

https://figshare.com/articles/dataset/readme_figshare_gmst_txt/8137748?backTo=/collections/Global_mean_temperature_reconstructions_over_the_Common_Era/4507043.

In the result section, we identify peaks in decennial temperature changes that are common for the two series. However, all subsequent analyses are based on the Moberg time series because they show the largest overall variance.

We obtained the $CO_2$ data from "Law_Dome_Ice_Core." The series run from the year 1 to 2004 (Meure et al. [2006](#)) and were extended with data from Mauna Loa, https://www.esrl.noaa.gov/gmd/ccgg/trends/.

We define four subperiods during the Common Era and use the first three periods as defined by Neukom et al. ([2019a](#), Extended data Fig [4](#)) and add a period for the industrial era. The four periods are the Roman warm period, 1–750 (RWP), the medieval period, 751–1350 (MED), the Little Ice Age, 1001–2000 (LIA), and the consolidation of the Industrial era, 1880–2019 (IND). In the following we use the term "decadal" for the time window of 11 years long. Eleven years enables us to identify a midpoint year.

## 3 Method

We calculated running average slopes in two ways. First, we used the $\beta$ - coefficient of the equation NHTA = $\beta \times$ time + $\alpha$ over 11, 21 and 51 consecutive samples. Second,

we used the slope as S = NHTA$_{t+n}$ - NHTA$_t$ where n is 11 to 71 years in steps of 10 years. The 51-year time window is used to represent the multidecadal periods in Wang et al. ([2022](#)). The difference between the two values at the end of the decadal and bi-decadal windows was used instead of the slope to have the possibility to encounter a larger spread. The first method will be named the β-method and the second method the difference method.

The minimum and the maximum slopes were then identified separately for the time windows of the series before 1880 (1–1880, 1876 years) and after 1880 (1881–2022, 134 years). For the NHTA we used the raw values. However, for the $CO_2$ data there were observations with similar values, so we added a small fraction of random numbers to the series to avoid singularities ($0.1 \times$ RAND(), where RAND() is the Excel random generator). The number of "large" positive and negative slopes for each of the time windows was identified by screening the two time series for slopes that were either less than $-x_{average} - 1\times$ standard deviation (SD) or more than $x_{average} + 1\times$ SD. The 95% confidence interval is ±0.00115.

To set the maximum and minimum values into context, we constructed histograms for the distribution of slopes before and after 1880. Since there are more slopes before 1880, we centered, detrended and normalized the distributions to unit standard deviation to make them comparable and depicted them in the same graph.

We applied LOESS smoothing to the raw data. Its parameter (f) is the fraction of the time series length used as running average window, and parameter (p) is the degree of polynomial function used for smoothing. Since we always use $p = 2$, we use the nomenclature LOESS(f) for the smoothing degree. When a series is both detrended and smoothed, we use the nomenclature LOESS (0.x – 0.y) where the series first are slightly smoothed LOESS (0.x) to avoid high frequency noise and thereafter detrended by subtracting a strongly smoothed L (0.y) series. We disentangled the NHTA series into component series that may be the result of different mechanisms by applying LOESS smoothing. Our aim is to focus on decadal and multidecadal variations.

We calculated cycle periods by depicting two versions of the detrended, centered and normalized NHTA series in a phase plot, the original series on the x-axis and the series shifted 5 years backward on the y-axis. When the trajectory between points in the phase plot closes and the cumulative angle relative to the origin becomes $2\pi$, one cycle period is identified. (The "cumulative angle" method Seip and Grøn ([2018](#))).

For $CO_2$, we disentangled the series as for the GTA data with one exception. The curve indicating decadal movements was obtained only for the period 1 to 1880 because the last rapid growth in $CO_2$ concentration after 1880 was masked by the decadal movements in the 1–1880 period.

Finally, we examined the running average volatility of the temperature series by calculating the running standard deviation over 11 consecutive years. All calculations were made in Excel and Sigma Plot. All data and all calculations are available from the first author.

# 4 Results

We first show results for the NHTA and the $CO_2$ series for the period 1–2019. Thereafter we embed the results in graphs showing the two temperature series NHTA and GTA for the four periods we have divided the Common Era in, RWP, MED, LIA, and IND. Third, we show how the maximum temperature changes related to sub periods identified in the literature and that have been examined for causal mechanisms. Last, we estimate cycle characteristics for the NHTA series.

## 4.1 Time series, NHTA, and $CO_2$ for the Common Era

Results for the NHTA and the $CO_2$ data are shown in Fig. 1a. The figure shows both the raw data, the data strongly smoothed to indicate millennial scale changes, and the residuals between the raw and the strongly smoothed data to indicate centennial variations (upper curve). The residuals were also smoothed, $f = 0.1$–$0.2$ to reduce high frequency variability. The lower curve in Fig. 1a shows a smoothed curve for the volatility in the temperature series. It is seen that the volatility decreases during the industrial era. Figure 1b shows the running slopes over 11-year periods and a LOESS(0.4) smoothed version, (bold curve).

We estimated the increase/decrease in NHTA and $CO_2$ during the periods 1 to 1880 and 1881 to 2019. The results are summarized in Tables 1 and 2. We first show the results calculated by the difference method. For NHTA, Table 1 shows average, maximum and minimum slopes calculated for 11, 21 and 51 years, but for $CO_2$, slopes over 11 years give sufficient information to conclude that the slopes during the industrial era are much steeper than during the pre-industrial era. Table 2 shows comparable results to those in Table 1, but calculated with the β – method and only for the 11-year time windows.

The maximum changes in NHTA over 11-, 21-, and 51-year periods are shown with drop lines for the dates in Fig. 1a and c shows the corresponding data for $CO_2$.

The NHTA series and the $CO_2$ series correlate reasonably with each other,

$$NHTA = -2,985 + 0,00937 \times CO_2, r = 0.57, p < 0.001, n = 2022 \tag{1}$$

For NHTA, the decadal changes are similar before and after the start of the industrial era. However, whereas decreasing and increasing slopes (values outside $x \pm 1$ SD) were about equal in numbers before 1880 (ratio of positive to negative slopes 1.02), there were more positive slopes than negative slopes after 1880 (ratio of positive to negative slopes 3.9), Table 1, two right columns. With slopes estimated over 21 years, the ratio between positive and negative values is 1.03 during pre-industrial time, and 6.22 during the industrial era.

For $CO_2$, the ratio between positive and negative slopes during pre-industrial time was 0.7. During industrial time there were no significant negative slopes, but 95 positive slopes.

## 4.2 Temperature series, NHTA, and GTA, for the four periods RWP, MED, LIA, and IND

We examine the ordinary linear regression (OLR) correlations for the NHTA and the GTA series during four periods in the Common Era. When the full series for NHTA and GTA are slightly LOESS(0.1) smoothed, the correlation between NHTA and GTA is high $R \approx 0.8$. However, it is the variability in temperature during the LIA that dominates the good correlation. Separately, the RWP and the MED periods have correlation coefficients around $R = 0.2$ with optimal LOESS smoothing, whereas the LIA shows an optimal correlation of $R = 0.8$–$0.9$, Fig. 2a. We detrend the series using LOESS(0.4) and LOESS (0.8) and obtain the trends in Fig. 2b. For the periods, we then get regression coefficients $R = 0.33$ for the RWP, $R = -0.09$ for the MED, $R = 0.45$ for the LIA, and $R = 0.26$ for the IND, Fig. 2c, d, e, and f.

We compare the dates when maximum slopes are identified to events that have been explored and explained in the literature within each of the periods RWP, Fig. 2c, MED, Fig. 2d, LIA, Fig. 2e, and IND, Fig. 2f. The figures show the two temperature series NHTA and GTA, short time windows identified as events that can have been given causal explanations for why they occurred (horizontal bars), and crosses that identify maximum slopes over 11, 21, and 51 years. Droplines identify peaks in temperature that are common for the NHTA and GTA.

The distribution of slopes during pre- and industrial times are shown in Fig. 3a and b for NHTA. We depict the histograms for the difference method, $X_{t+11}-X_t$ in Fig. 3a and for the β – coefficient in Fig. 3b. For the $CO_2$ distribution it is sufficient with the $CO_{2\,t+11}$ -$CO_{2\,t}$ calculations since the differences in the patterns are easily seen in the same histogram, Fig. 3c. In Fig. 3d, we compare slopes for NHTA calculated by the two methods. The two measures for the slope are close ($R^2 = 0.78$).

The scatter plots and their regression against time for the time window with the maximum slopes during the pre-industrial time are shown in Fig. 4a and the time window for maximum slopes during the industrial time are shown in
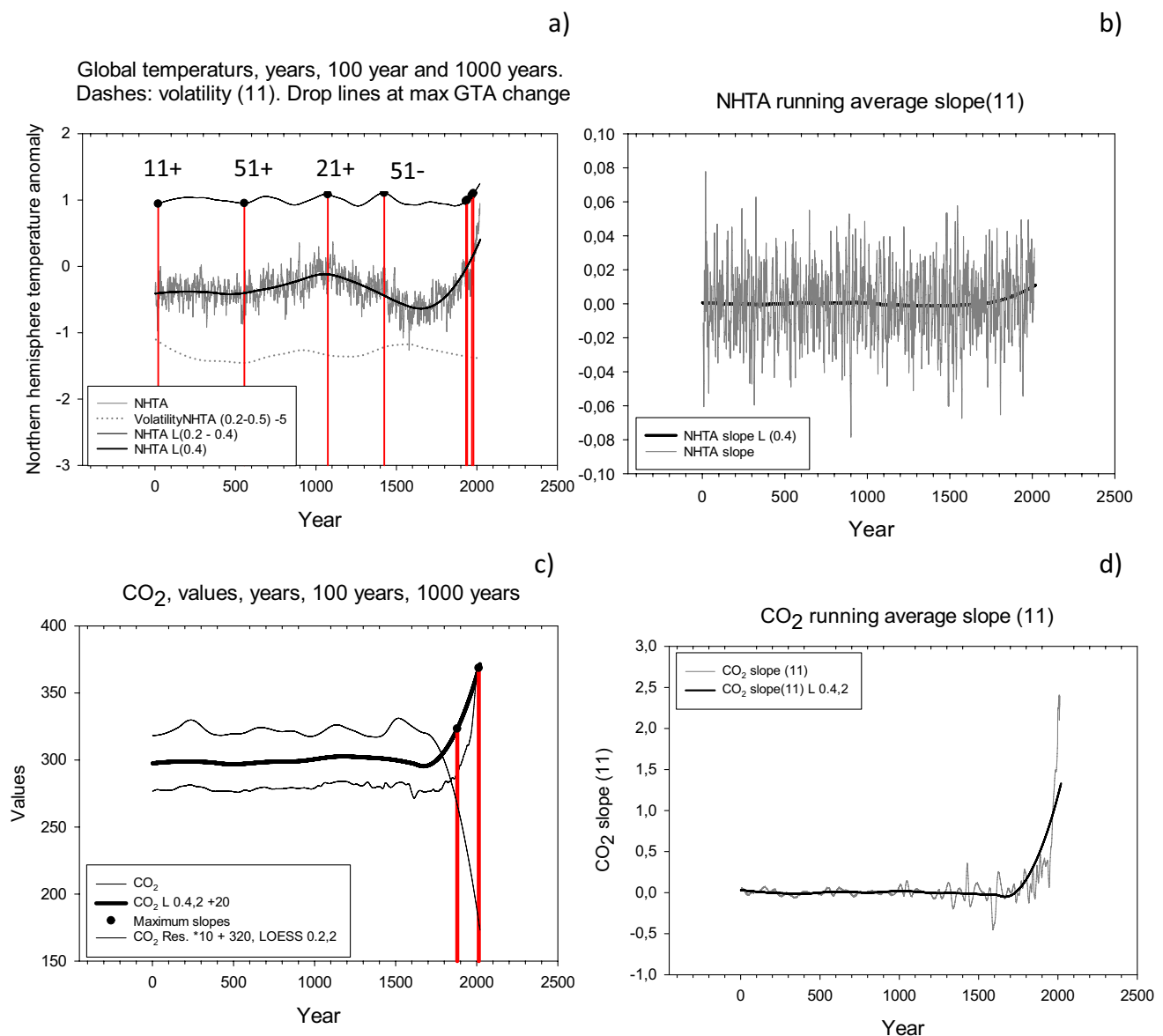
a)

Global temperatures, years, 100 year and 1000 years.
Dashes: volatility (11). Drop lines at max GTA change



b)

NHTA running average slope(11)



c)

$CO_2$, values, years, 100 years, 1000 years



d)

$CO_2$ running average slope (11)



**Fig. 1** The Northern Hemisphere mean temperatures year 1 to 1880 extended with the global mean temperature 1979 to 2019. **a** Temperature anomalies, from bottom: Lower dashed curve shows running smoothed temperature variability over 11 years. Dark grey curve shows annual values, bold curve suggests millennial temperature changes and upper curve suggests centennial temperature changes. Vertical lines at years 20, 1074 show midpoint dates for 11- and 21-years max slopes for pre-industrial period. Vertical lines at years 1933, 1969 show midpoint dates for 11- and 21-years max slopes for industrial period. Vertical lines for years 555 and 1425 show midpoint dates for min and max slopes for 51 years window. **b** Running average slopes, $n = 11$, years 1 to 2019. The smoothed line shows the raw data LOESS(0.4) smoothed. **c** Carbon dioxide time series year 1 to 2019. Lower curve shows annual values, middle curve suggests millennial changes and upper curve decennial to centennial changes. Vertical lines show midpoint dates for 11 years max slopes for pre- and industrial times. **d** $CO_2$ running average slope 1–2019. The thick line shows a L(0.4) smoothed version

Fig. 4b, lower scattergram. In Fig. 4b, we have in addition shown the scatterplot for the observations during the last period recorded, 2009 to 2019, upper scattergram.

The size of the time window matters for the IND period 1881– 2019, whereas the maximum slopes are almost constant for the pre-industrial time, Fig 4c (Note that the last 5 and ten 10 years are not included for the decennial

and the bi-decadal respective time windows.) For time windows greater than about 20 years, the maximal slopes during the industrial era become larger than the slopes before 1880. The black dashed curve shows slopes for a second order polynomial curve fitted to NHTA 1881 to 2019 for increasing time windows. The ratio of significant positive slopes to negative slopes are much greater

**Table 1** Decadal and multidecadal changes in NHTA and $CO_2$ during pre-industrial time, year 1 to 1880, and during industrial time 1881 to 2019. Calculations with the difference method. Significant changes are those that exceed x $\pm$ 1 SD. RWP Roman warm period, MED medieval period, LIA Little Ice Age

| Time series | Period | Window (years) | average change (°C period$^{-1}$) | Min Change/°C period | Max change/°C period | #Significant neg. changes | #Significant pos. changes |
|---|---|---|---|---|---|---|---|
| GTA | All 1–2019 | 11 | 0.003 | | | | |
| | Pre-industrial 1–1880 | 11 | 0.00±0.22 | −0.86, year 900 | 0,86, year 20; RWP | 267 | 273 |
| | | 21 | 0.003±0.23 | −0.69, year 1064 | 0.96, year 1074, MED, LIA | 330 | 339 |
| | | 51 | 0.00±0.24 | −0.76 year 1425 | 0.81, year 555 RWP | 248 | 232 |
| | Industrial 1881–2019 | 11 | 0.09± 0.16 | −0.6, year 1944 | 0.68, year 1933 | 9 | 35 |
| | | 21 | 0.18±0.21 | −0.16, year 1948 | 0.94, year 1969 | 9 | 56 |
| | | 51 | 0.39±0.27 | 0.02, year 1940 | 1.41, year 1979 | 4 | 43 |
| $CO_2$ | All 1–2019 | | 0.63±0.28 | −4.53, | 2.407 year 2008 | | |
| | Pre-industrial 1–1880 | 11 | 0.07±0.28 | −0.453, year 1592 | 1.79, year, 1880 | 18 | 2 |
| | Industrial 1881–2019 | 11 | 13.0±0.70 | 0.65, year 1945 | 24.07, year, 2008 | 0 | 95 |

**Table 2** Decadal changes in NHTA and $CO_2$ during pre-industrial time, year 1 to 1880, and during industrial time 1881 to 2019. Calculation with ordinary linear regression method, the β -method. Significant changes are those that exceed x $\pm$ 1 SD. RWP Roman warm period, LALIA Late antique little ice age

| Time series | Period | window | average change | Min change | Max change | #Significant neg. changes | #Significant pos. changes |
|---|---|---|---|---|---|---|---|
| GTA | All 1–2019 | | 0.01±0.022 | | | | |
| | Pre-industrial 1–1880 | 11 | 0.00±0.022 | −0.85, year 289 | 0.68, year 672 RWP (LALIA) | 272 | 265 |
| | Industrial 1881–2019 | 11 | 0.227±0.336 | −0.56, year 1912 | 0.55, year 2015 | 14 | 29 |

after 1880 than before and may stabilize on a ratio of 10 to 12, Fig. 4d.

Plotting the slopes, $T_{t+11} - T_t$, T is temperature, versus time, we found that after 1971 there is only one year that show negative decadal slopes, Fig. 4e. LOESS (0.1) smoothing the NHTA series, 16 cycle periods can be identified visually, and confirmed with the "cumulative angle" method (Seip and Grøn 2018).

## 5 Discussion

A frequent statement in the global warming debate is that the decadal increase in global temperature, GTA, has never been stronger than during the last decade, e.g., Graver and Stenseth (2020). We found that the pre-industrial era showed steeper increases in NHTA than during the industrial era. However, the frequency of positive, steep slopes (greater than the average, NHTA +1 Sta. Dev.) was much higher during the industrial era than during the pre-industrial era. Table 1 shows that the conclusion is strengthened when we use 21-year time windows. For time windows greater than about 20 years, the slopes during the industrial era become steeper than the slopes during the pre-industrial era. Thus, our hypothesis **H1** was supported, there are steeper temperature changes for decadal time windows 11 to ≈ 20 years during preindustrial times.

The histograms in Fig. 3a and b showed that the pre-industrial and industrial eras showed almost similar slopes in decadal NHTA changes. With both methods for calculating the slopes, the distribution of slopes for the industrial era is skewed towards larger slopes, but the maximum slopes are greater for the preindustrial era.

### 5.1 Increases in NHTA before and after 1880

We found that there would be periods for 20 years or less where non-anthropogenic factors and man induced aerosols (Hansen et al. 2022) could increase NHTA as fast as during the industrial era. However, there are two indications that the maximum increase in NHTA, although smaller, is more persistent during the industrial era. *First*, the regressions comparing max slopes during the period 1881 to 2019 have much less variability expressed by the explained variance, $R^2$, for the last years 2009 to 2019 than for the earlier period around 1933 (1928-1938) that was identified as
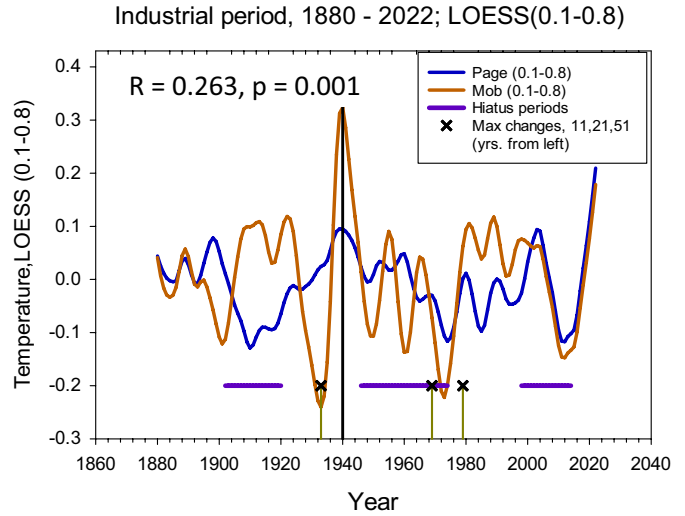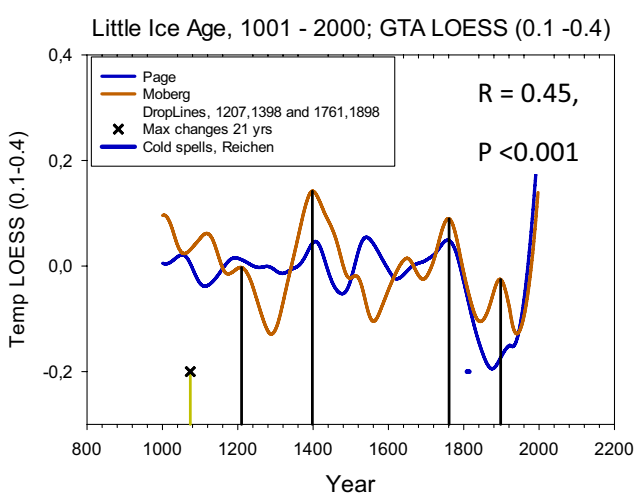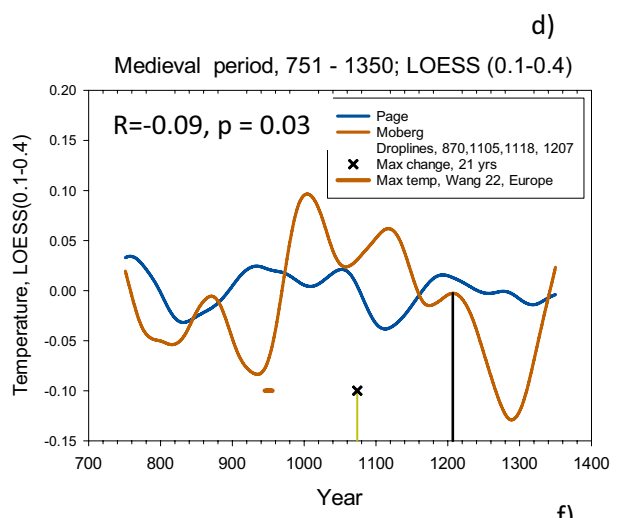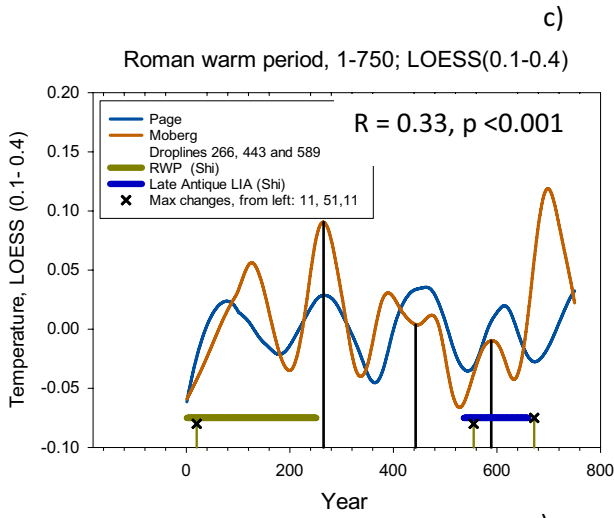
a)

LOESS(x) smoothing temperatures during
periods of the common era



b)

Trends, Roman,L(0.4); Medival,L(0.4); LIA,L(0.4); IND,L(0.8)



c)

Roman warm period, 1-750; LOESS(0.1-0.4)



d)

Medieval period, 751 - 1350; LOESS (0.1-0.4)



e)

Little Ice Age, 1001 - 2000; GTA LOESS (0.1 -0.4)
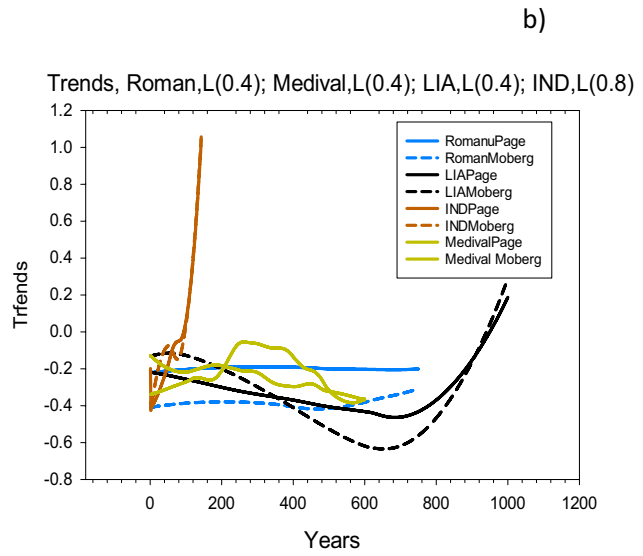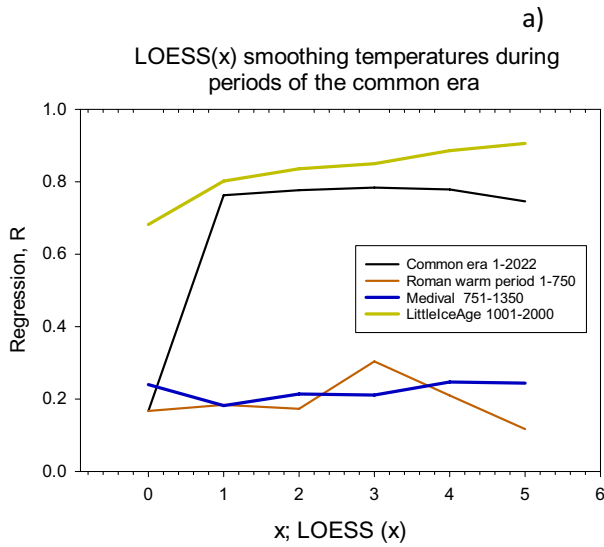


f)

Industrial period, 1880 - 2022; LOESS(0.1-0.8)

◄**Fig. 2** Comparing Common Era datasets for the Northern Hemisphere, NHTA, by Moberg et al. (2005) and for the globe by PAGE2k (2017). **a** Ordinary linear regression, R, between periods in the NHTA and PAGE temperature series with increasing LOESS smoothing, LOESS (x), see text. The periods are the Roman warm period, RWP, 1–750; the Medieval period, MED, 751–1350; the Little Ice Age, LIA, 1001–2000; and the industrial period, IND, 1881–2019. **b** Trends removed from the four periods. LOESS(0.04) trend from the three first periods, LOESS(0.8) trend removed from the IND. **c** The RWP, comparing L(0.2–0.4) smoothed and detrended series. For three years GTA and NHTA show peaks at the same time (droplines). The bold horizontal lines show sub periods identified by Shi et al. (2022). Crosses show the years of max temperature changes with two methods (Diff and β method, this study). **d** The MED, comparison of NHTA and GTA series as in (**c**). For 1 year, GTA and NHTA show peaks at the same time (droplines). The bold horizontal line shows max temperature in the Page series identified by Wang et al. (2022, Fig 2e). The cross shows a year with max temperature change (this study), **e** LIA, comparison of NHTA and GTA series as in (**c**). For 4 years, GTA and NHTA show peaks at the same time (droplines). The horizontal bold line shows a cold spell period identified by Reichen et al. (2022). **f** IND. comparing L(0.2–0.8) smoothed and detrended series. After about 1940, the two series correspond fairly well. The horizontal bold lines show hiatus periods identified by Yao et al. (2016). The crosses show max temperature changes (this study)

having maximum decadal slope, Fig. 4b. S*econd*, the cigar formed shape in Fig. 3d describing the relation between the two definitions of slopes is narrower at high slopes showing that the two methods then give more similar values for the slopes. This, again, would indicate that the values increase more persistently and have fewer deviating years at high values of the slopes.

We found that max decadal temperature changes occurred during all periods (MED and LIA overlap). Thus, our hypothesis, **H2**, that most maximum slopes would occur during the LIA, was not supported. Maximum changes over decadal and multidecadal time windows occurred during all periods, and three of the slopes occurred during the RWP and in association with sub-periods identified by Shi et al. (2022).

## 5.2 Seven possible explanations for differences in GTA slopes during the pre-industrial and industrial periods

We found that there would be periods up to about 20 years where non-anthropogenic and anthropogenic factors could increase the global temperature during the pre-industrial era as fast as during the industrial period. However, the increases in NHTA over periods longer than about 20 years are unique for the greenhouse gas era.

Below, we discuss seven candidate variables that may explain variability in NHTA changes. However, some factors may act primarily as causal agents for other factors. Thereafter, we discuss the four periods. We examine whether any of the decadal changes we have identified,

min or max, can be related to events that are discussed in the literature for any of the periods.

**1. Volcanism** Volcanism would cause a cooling of the GTA for a certain period and then a subsequent warming to "normal" temperature defined by an equilibrium between heat emission and heat sequestration at the top of the atmosphere. Volcanism may impact GTA changes over decadal times (Anchukaitis et al. 2017), but the effects will also depend upon the frequency of eruptions (Stoffel et al. (2022), and where they occur (Wang et al. (2022).

**2. Aerosols** The most prominent source of aerosols in the atmosphere/stratosphere is from volcanism. However, recently, Hansen et al. (2022, p.11) suggest that aerosols from gras and forest fires (Seip and Wenstøp 2006, pp. 365-366), dust from wind and droughts and marine aerosols have reduced insolation considerably and thus contributed to a slower increase in global warming by $CO_2$ than it would have been without aerosol emissions.

**3. Solar forcing** Solar forcing has been found to be weak relative to the NHTA, except possibly over bi-centennial scales (Vieira et al. 2011, Anchukaitis et al. 2017).

**4. Heat exchange within the oceans, and between the oceans, land, and the atmosphere** There is little information on the heat exchange or ocean dynamics before about 1950. However, some ocean variability series have been extended backwards in time, Sun et al. (2021). Wang et al. (2009) suggested that there is a circular causal sequence between the North Atlantic oscillation (NAO), ocean oscillations in the Pacific, the stratosphere and then NAO again. Yao et al. (2017) suggest that changes in ocean temperature in the Pacific and the Atlantic may explain periods with enhanced global warming, and Wu et al. (2019) attribute about 30 % of the changes in multi decadal global mean surface air temperature to Atlantic and Pacific temperature variability, i.e., vertical ocean movements between ocean layers. Recently, Tsubouchi et al. (2020) have shown that a mean ocean heat transport has occurred into the Northern Seas and the Arctic Ocean over a 20-year period. Thus, both vertical and horizontal ocean water movements may play a role for variability in the NHTA.

**5. $CO_2$ exchange within the oceans and between oceans, land, and the atmosphere** The natural changes may be due to sequestration and emissions of $CO_2$ from the oceans or from land (Feely et al. 2017, Gruber et al. 2019a, Gruber et al. 2019b, Thompson et al. 2022). This again affects the concentration of $CO_2$ in the atmosphere and thus the variability in GTA.
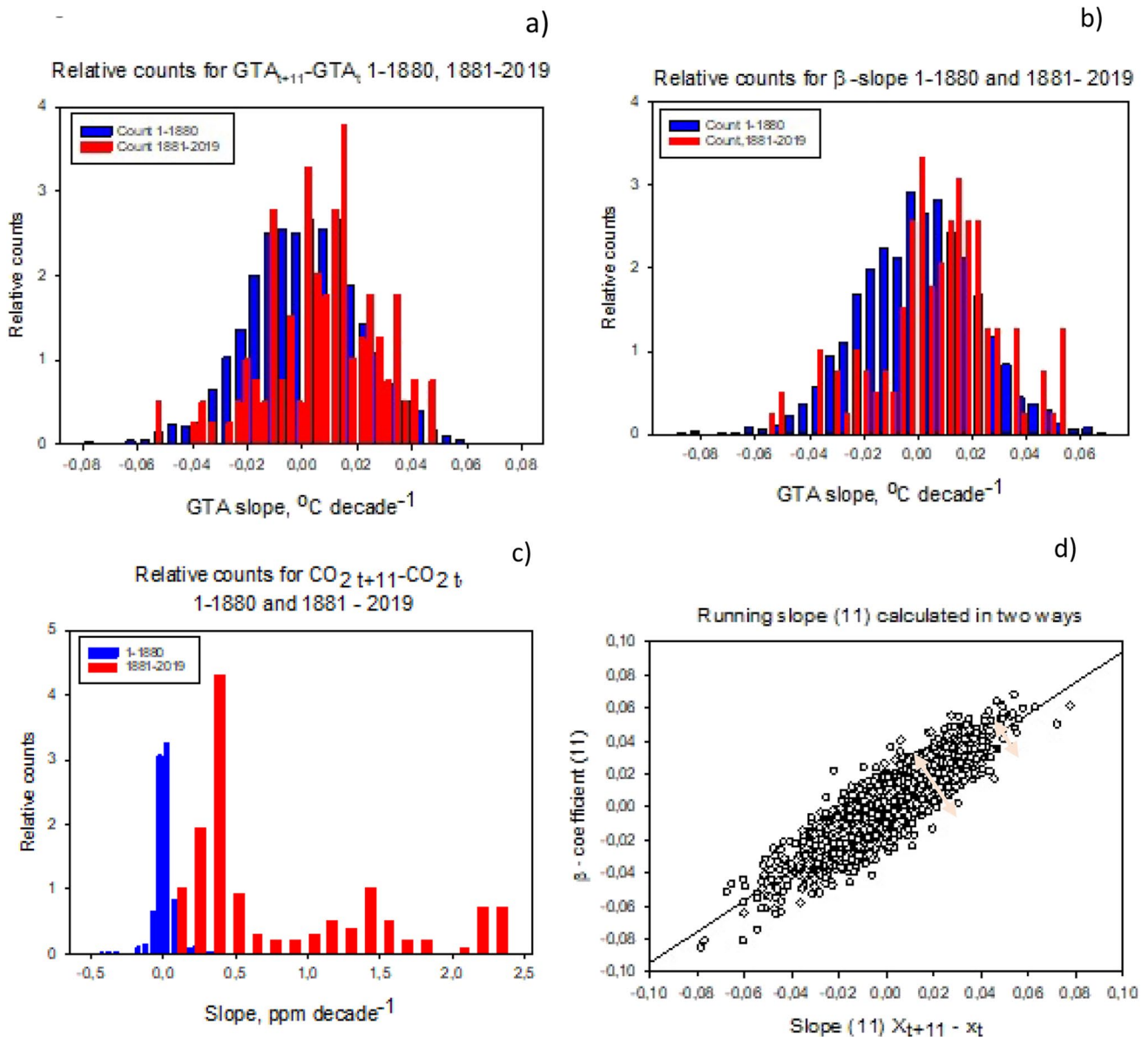
**Fig. 3** Histogram and scatter plot for NHTA-slopes, and histogram for $CO_2$ – slopes. **a** Slopes calculated as the difference $GTA_{t+11}$ – $GTA_t$ over running time windows of 11 years for the periods 1–1880 and 1881–2019. **b** Slopes (β – coefficients) calculated from regression line over running time windows of 11 years. There are 1876 slopes for the pre-industrial period 1-1880 and 134 slopes for the period 1881 to 2019, but the counts have been centered and normalized to unit standard deviation. **c** Histogram for $CO_2$ slopes calculated as the difference $CO_{2\ t+11}$ – $CO_{2\ t}$ over running time windows of 11 years. **d** Scatter plot for two methods for calculating slopes. Double arrows suggest width of scatterplot

**6. Greenhouse gases** Knowledge of $CO_2$ extends 800 million years back, but except for the last 200 years, the resolution in time is probably too low to detect significant changes in $CO_2$ over decadal or multidecadal time windows. Thus, large variations in $CO_2$ over centuries during paleoclimate records are probably not relevant for variations over decadal or multidecadal periods in historic time.

**7. Self-reinforcing mechanisms** Among self-reinforcing mechanisms is the melting of the Greenland ice -cover (Hand et al. 2020, Skagseth et al. 2020). As ice melts because of a triggering global warming, the surface albedo decreases due to a large open water and melt-pond fractions. We do not know the contribution to global heating from increased absorption of heat caused by a darker surface, but

during the recent interglacial period, 130,000–116,000 years before present, Arctic land surface temperatures were 4–5°C higher than recent industrial temperatures, and ice-loss was fast (Guarino et al. 2020). The present Arctic temperature is increasing faster than the average global warming (Screen et al. 2018).

## 5.3 The periods

The beginning and the length of the four periods RWP, MED, LIA, and IND are discussed in the literature. For the first three periods we used the definition proposed in Neukom et al. (2019b). We define the industrial revolution period as beginning in 1880, but basic industrial inventions occurred about 100 years before. The number in parentheses below refer to candidate causes listed above.

### 5.3.1 The Roman warm period

The Roman period has been assigned two subperiods by Shi et al. (2022), the Antique Roman warm period (1–250) and the Late Antique Little Ice Age (536–660). Figure 2c shows these two periods as red and blue horizontal lines. The warm period may be related to increased radiative forcing associated with weaker (relative to later) volcanic eruptions (1), increased insolation, reduced sea ice area (7), and increased upper ocean heat content (4).

### 5.3.2 The Medieval period

The summer peak temperature during the Medieval and the Little Ice Age periods has been compared by Wang et al. (2022) and shows that the peak temperatures occurred at about the same time in the Arctic, the North America and Europe. Figure 2d shows the period with peak temperature as a red horizontal line. The authors attribute the peak temperatures to internal (4) and external (1) forcings, the latter being more dominant at larger time and space scales.

### 5.3.3 The Little Ice Age period

The Little Ice Age has been assigned several winter cold spells, the most prominent being from 1808 to 1815 (Reichen et al. 2022). Figure 2e shows the "cold spell" period as a blue horizontal line. The authors attribute the winter cold spells to two tropical volcanic eruptions (1) and ocean variability (4). The effects caused by stratospheric aerosols emitted by the volcanoes triggered changes in snow cover and thus a decrease in the albedo (7). Ocean variability (4) was due to the weakening of sea level pressure (SLP) at the Islandic low (Reichen et al. 2022, p. 5) during the period 1808–1815. Furthermore, Chen et al. (2018) suggest that the 50–70 years Pacific multidecadal

variability (PDO) is instigated by persistent volcanic forcing during the Little Ice Age (1250–1850) (1).
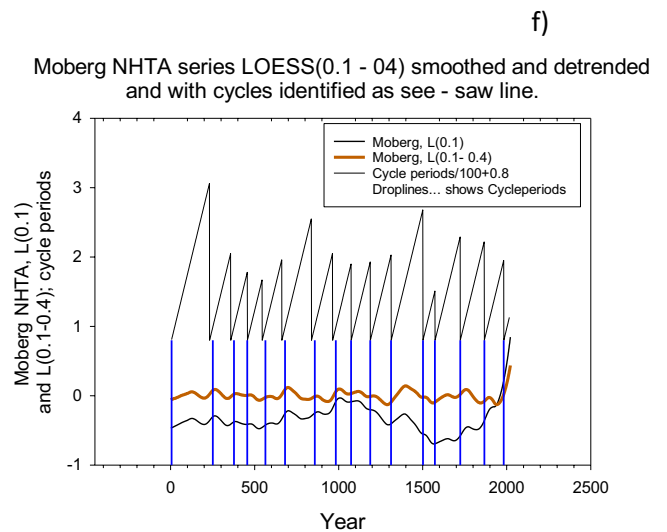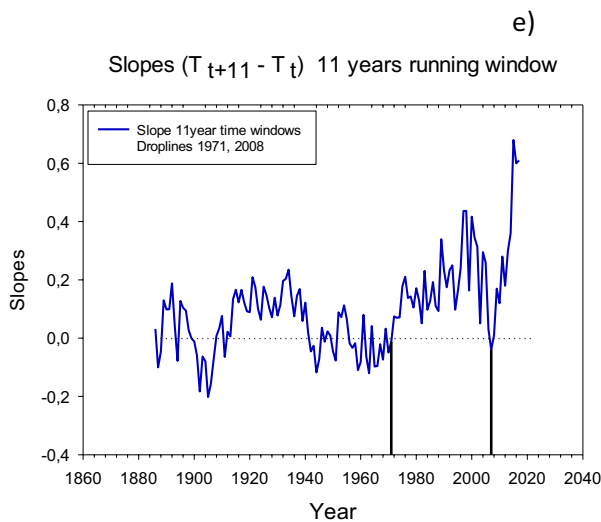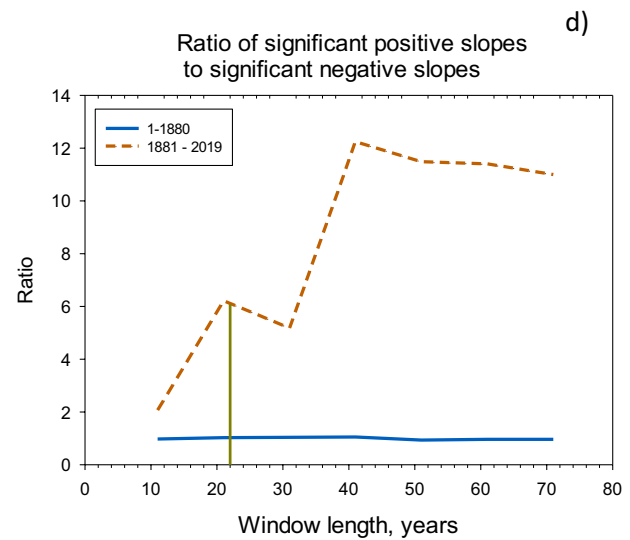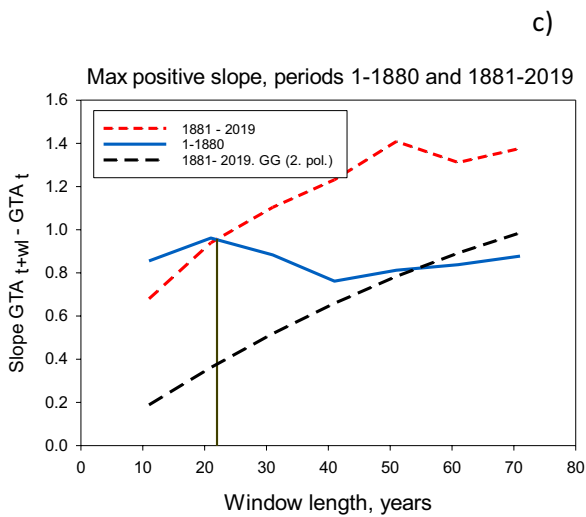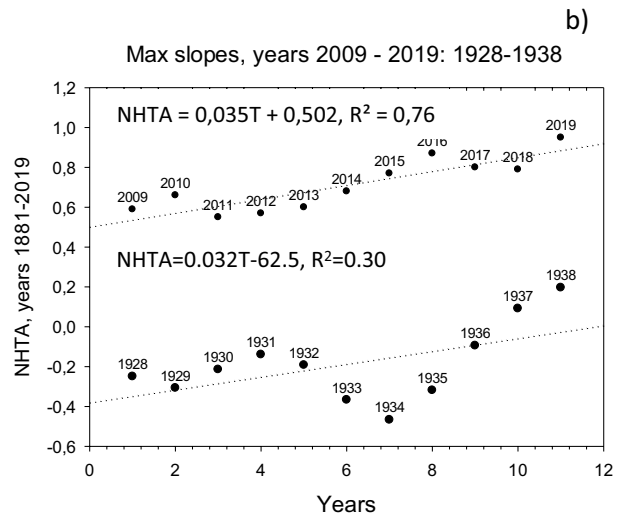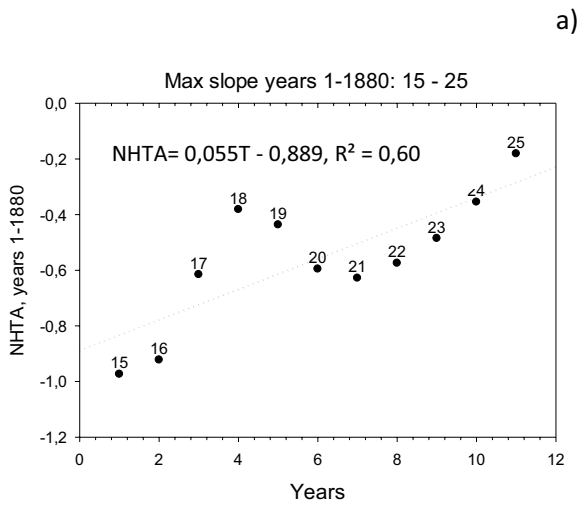
### 5.3.4 The industrial period (IND)

There is an overall sharp rise in NHTA during the IND, but there are also periods where the rise is damped or reversed, the hiatus periods. In Fig. 2f, the hiatus periods are shown as blue horizontal lines. The slowdown may be due absorption or transport of heat to the deep layers (101–300m) of the ocean (4), (Cheng et al. 2015, Figure 2, p. 3). The deep absorption again may be related to periods where El Niño ceases to be leading the Pacific decadal variation (PDV), Seip and Wang (2018). However, Wang et al. (2009) show that only when NAO's coupling with the Pacific increases, a climate shift will occur. Minimum average change in NHTA occurred during the period 1940 to 1948, that is during the second hiatus period. The maximum slopes occurred in-between the two first hiatus periods and the two next at the end of a hiatus period. If we let the smooth 2-order polynomial function represent warming by anthropogenic forces, then the net temperature changes is always less than during the pre-industrial era, Fig. 4c. The net maximum changes, the sum minus anthropogenic contributions, may be due to variabilities in the NAO and the Atlantic multidecadal Oscillation (AMO) (Lüdecke et al. 2022) and the AMOC (Seip and Wang 2022). There are only one period where the decadal temperature window shows a negative slope after 1971, Fig. 4f. Thus, even though a hiatus period is identified from 1999 to 2012, Trenberth and Fasullo (2013), anthropogenic warming cancels cooling by natural forces after 1971.

## 5.4 Robustness

Our results depend upon our choice of temperature series for the last 2020 years. There are other series available as well, and those series could be explored (Christiansen and Ljungqvist 2017). However, all series are based on proxy records, and we do not know if one is better than the other. A possible further approach could be to do detailed studies of periods with high global temperature increases, first to establish that they are real and next to identify the factors that caused the strong increase.

## 5.5 Causes for variability in the Common Era temperature series

All factors 1 to 7 can potentially act both during the pre-industrial and the industrial period. However, the probability that a factor, like volcanism, would exert a strong force, or that several factors could act in concert and strengthen

a)



Max slope years 1-1880: 15 - 25

$NHTA = 0.055T - 0.889$, $R^2 = 0.60$

b)

Max slopes, years 2009 - 2019: 1928-1938

$NHTA = 0.035T + 0.502$, $R^2 = 0.76$

$NHTA = 0.032T - 62.5$, $R^2 = 0.30$

c)

Max positive slope, periods 1-1880 and 1881-2019

d)

Ratio of significant positive slopes to significant negative slopes

e)

Slopes ($T_{t+11} - T_t$) 11 years running window

f)

Moberg NHTA series LOESS(0.1 - 04) smoothed and detrended and with cycles identified as see - saw line.

warming or cooling effects would be higher during the long preindustrial period (1876 years) than during the industrial period (134 years).

A support for the role of ocean variability for decadal and multidecadal variabilities in NHTA and GTA is that there seems to be common cycle periods for the detrended

◄**Fig. 4** NHTA change around midpoint years that gave maximum changes over a 11-year period. Note that the change is calculated as the difference in NHTA values between the last and the first year in the periods. **a** Pre-industrial period 1–1880, max slope around the year 20 (15–25). **b** Industrial period 1881–2019. The decadal slope is shown for the year with steepest slope, 1933 (1928–938) and for the year 2014 (2009–2019). **c** Slopes as a function of window length for pre- and post-1880. The black line shows maximum slopes for a second order polynomial function fitted to the NHTA for the industrial period and representing the effects of GHG. **d** Ratio between significant positive slopes and significant negative slopes for pre- and post-1880. Droplines show crossing point at year 22. **e** Running 11 years window for temperature slopes $T_{t+11} - T_t$. **f** NHTA series LOESS(0.1–0.4) smoothed and detrended. See-saw curve shows cycle periods

and LOESS(0.1–0.4) smoothed NHTA and GTA series of 7, 9–12 years, 14 years, 17–18 years, and 20–23 years. Seip et al. (2019) found significant cycles of 7, 13, and 20 years for the AMOC, AMO, and NAO.

With a high-resolution lead-lag method, Seip et al. (2018), we identified eight common cycle periods with an average length of 251 ± 110 years for the LL(0.2) smoothed NHTA series and 16 cycle periods with an average length of 131 ± 39 years for LL(0.1) smoothed series (16 cycles shown in Fig. 4f.) Although not perfect, the cycle periods can also be identified in the time series representation. We believe that among the potential mechanisms that could cause persistent cycles and function as a pacemaker for cycle periods is ocean variability series. Ocean variability series show series with several cycle periods superimposed, e.g., Arzel and Huck (2020), and Arzel et al. (2018) and both the Arzel papers and Seip and Grøn (2019b) offer explanations for how they are created. Thus, hypothesis **H3**, was only partially supported. Several studies included ocean variability to explain variabilities in NHTA and GTA, but also added potential factors like volcanism. Such additional factors may contribute to decadal and multidecadal variations, but it is less likely that they can function as pacemakers for centennial or multicentennial variations.

**Environmental policy consequences** The public often expresses concerns over annual temperature events, like very cold or very warm years. However, the important issue that should be communicated is that the cold periods are, on average, still a little warmer than previous cold years and the warm periods are a little warmer and last longer than previous warm periods. Periods less than about 20 years with steep changes in temperatures were as frequent during the pre-industrial period as they are now, but there are many more periods with steep increases in temperature than periods with steep decreases in temperature.

# 6 Conclusion

Extreme decadal and multidecadal changes in Northern Hemisphere temperature anomaly during time windows less than about 20 years were as steep during the first part of the Common Era, years 1–1880, as during the last, industrial era. However, decadal and multidecadal warming periods were more frequent during the latter period. Decadal and multidecadal variabilities in the IND period are superimpositions on a persistent increase caused by increasing greenhouse gas concentrations, e.g., $CO_2$, in the atmosphere. Subtracting the effects of green house gases, temperature variabilities after 1880 were always less than during the preindustrial era. After 1971, there is only one year (2008) where the decadal period shows a negative slope. The year 2008 (a year in the last hiatus period) is also designated as a tipping point for the snow cover in the Tibetan plateau as well as related to other tipping points. Furthermore, it is the year with maximum changes in $CO_2$ during the IND era. Of the seven candidate causes for decadal or multidecadal changes in NHTA, we suggest that our results support variability in the ocean as a dominating cause during the Common Era because the NHTA shows signals that a pace maker mechanism is present.

## Declarations

# References

Anchukaitis KJ, Wilson R, Briffa KR, Buntgen U, Cook ER, D'Arrigo R, Davi N, Esper J, Frank D, Gunnarson BE, Hegerl G, Helama S, Klesse S, Krusic PJ, Linderholm HW, Myglan V, Osborn TJ, Zhang P, Rydval M et al (2017) Last millennium Northern Hemisphere summer temperatures from tree rings: Part II, spatially resolved reconstructions. Quat Sci Rev 163:1–22

Arzel O, Huck T (2020) Contributions of atmospheric stochastic forcing and intrinsic ocean modes to North Atlantic Ocean Interdecadal variability. J Clim 33(6):2351–2370

Arzel O, Huck T, de Verdiere AC (2018) The internal generation of the Atlantic Ocean interdecadal variability. J Clim 31(16):6411–6432

Chen D, Wang HJ, Sun JQ, Gao Y (2018) Pacific multi-decadal oscillation modulates the effect of Arctic oscillation and El Nino southern oscillation on the East Asian winter monsoon. Int J Climatol 38(6):2808–2818

Cheng LJ, Zheng F, Zhu J (2015) Distinctive ocean interior changes during the recent warming slowdown. Sci Rep 5

Christiansen B, Ljungqvist FC (2017) Challenges and perspectives for large-scale temperature reconstructions of the past two millennia. Rev Geophys 55(1):40–96

Feely RA, Wannimkhof R, Landschützer P, Carter BR, Triñaes JA (2017) Global ocean carbon cycle. State of the climate 2016. Bull Amer Meteo 98:S89–S92

Graver HP, Stenseth NC (2020) Science, climate change and their consequences (Vitenskap, klimaendringer og deres konsekvenser). Aftenposten. Oslo, Aftenposten: 1, p 29

Gruber N, Clement D, Carter BR, Feely RA, van Heuven S, Hoppema M, Ishii M, Key RM, Kozyr A, Lauvset SK, Lo Monaco C, Mathis JT, Murata A, Olsen A, Perez FF, Sabine CL, Tanhua T, Wanninkhof R (2019a) The oceanic sink for anthropogenic CO2 from 1994 to 2007. Science 363(6432):1193-+

Gruber N, Landschutzer P, Lovenduski NS (2019b) The variable Southern Ocean carbon sink. Ann Rev Mar Sci 11:159–186

Guarino MV, Sime LC, Schroeder D, Malmierca-Vallet I, Rosenblum E, Ringer M, Ridley J, Feltham D, Bitz C, Steig EJ, Wolff E, Stroeve J, Sellar A (2020) Sea-ice-free Arctic during the Last Interglacial supports fast future loss. Nat Clim Change 10(10):928–932

Hand R, Bader J, Matei D, Ghosh R, Jungclaus JH (2020) Changes of decadal SST variations in the Subpolar North Atlantic under strong CO2 forcing as an indicator for the ocean circulation's contribution to Atlantic multidecadal variability. J Clim 33(8):3213–3228

Hansen JE, Sato M, Simons L, Nazarenko LS, Von Schuckmann K, Loeb NG, Osman MB, Kharecha P, Jin Q, Tselioudis G, Lacis A, Ruedy R, Russell R, Cao J, Li L (2022) Global warming in the pipeline. https://arxiv.org/abs/2212.04474

Lenssen NJL, Schmidt GA, Hansen JE, Menne MJ, Persin A, Ruedy R, Zyss D (2019) Improvements in the GISTEMP uncertainty model. J Geophys Res Atmos 124(12):6307–6326

Lüdecke H-J, Cina R, Dammschneider H-J, Lüning S (2022) Decadal and multidecadal natural variability in European temperature Ägeri, Institute for Hydrography. Geoecol Clim Sci 27

Meure CM, Etheridge D, Trudinger C, Steele P, Langenfelds R, van Ommen T, Smith A, Elkins J (2006) Law dome CO2, CH4 and N2O ice core records extended to 2000 years BP. Geophys Res Lett 33(14)

Moberg A, Sonechkin DM, Holmgren K, Datsenko NM, Karlen W (2005) Highly variable Northern Hemisphere temperatures reconstructed from low- and high-resolution proxy data. Nature 433(7026):613–617

Neukom R, Barboza LA, Erb MP, Shi F, Emile-Geay J, Evans MN, Franke J, Kaufman DS, Lucke L, Rehfeld K, Schurer A, Zhu F, Bronnimann S, Hakim GJ, Henley BJ, Ljungqvist FC, McKay N, Valler V, Von Gunten L, Consortium PK (2019a) Consistent multidecadal variability in global temperature reconstructions and simulations over the Common Era. Nat Geosci 12(8):643–649

Neukom R, Steiger N, Gomez-Navarro JJ, Wang JH, Werner JP (2019b) No evidence for globally coherent warm and cold periods over the preindustrial Common Era. Nature 571(7766):550–554

PAGE2k C (2017) Data descriptor: a global multiproxy database for temperature reconstructions of the Common Era. Scientific data. P. k. consortium, nature.com scientific data. Scientific Data 4:170088. https://doi.org/10.1038/sdata.2017.88

Reichen L, Burgdorf AM, Bronnimann S, Franke J, Hand R, Valler V, Samakinwa E, Brugnara Y, Rutishauser T (2022) A decade of cold Eurasian winters reconstructed for the early 19th century. Nat Commun 13(1)

Screen JA, Deser C, Smith DM, Zhang XD, Blackport R, Kushner PJ, Oudar T, McCusker KE, Sun LT (2018) Consistency and discrepancy in the atmospheric response to Arctic sea-ice loss across climate models. Nat Geosci 11(3):155–163

Seip KL, Grøn Ø (2019a) Cycles in oceanic teleconnections and global temperature change. Theor Appl Climatol 136:985–1000

Seip KL, Grøn Ø (2019b) On the statistical nature of distinct cycles in global warming variables. Clim Dyn 52:7329–7337

Seip KL, Wenstøp F (2006) A primer on environmental environmental decision-making. In: An integrative quantitative approach. Springer Verlag, Berlin

Seip KL, Wang H (2018) The hiatus in global warming and interactions between the El Nino and the Pacific decadal oscillation: comparing observations and modeling results. Climate 6(3)

Seip KL, Gron O, Wang H (2018) Carbon dioxide precedes temperature change during short-term pauses in multi-millennial palaeoclimate records. Palaeogeogr Palaeoclimatol Palaeoecol 506:101–111

Seip KL, Gron O, Wang H (2019) The North Atlantic Oscillations: cycle times for the NAO, the AMO and the AMOC. Climate 7(3)

Seip KL, Wang H (2022) The North Atlantic oscillations: lead–lag relations for the NAO, the AMO, and the AMOC—a high-resolution lead–lag analysis. Climate 10(5):63

Shi F, Sun C, Guion A, Yin QZ, Zhao S, Liu T, Guo ZT (2022) Roman Warm Period and Late Antique Little Ice Age in an earth system model large ensemble. J Geophys Res-Atmos 127(16)

Skagseth O, Eldevik T, Arthun M, Asbjornsen H, Lien VDS, Smedsrud LH (2020) Reduced efficiency of the Barents Sea cooling machine. Nat Clim Change 10(7):661–666

Stoffel M, Corona C, Ludlow F, Sigl M, Huhtamaa H, Garnier E, Helama S, Guillet S, Crampsie A, Kleemann K, Camenisch C, McConnell J, Gao CC (2022) Climatic, weather, and socio-economic conditions corresponding to the mid-17th-century eruption cluster. Clim Past 18(5):1083–1108

Sun C, Zhang J, Li X, Shi CM, Gong ZQ, Ding RQ, Xie F, Lou PX (2021) Atlantic Meridional Overturning Circulation reconstructions and instrumentally observed multidecadal climate variability: a comparison of indicators. Int J Climatol 41(1):763–778

Thompson AJ, Zhu J, Poulsen CJ, Tierney JE, Skinner CB (2022) Northern Hemisphere vegetation change drives a Holocene thermal maximum. Sci Adv 8(15)

Trenberth KE, Fasullo JT (2013) An apparent hiatus in global warming? Earths Future 1(1):19–32

Tsubouchi T, Vage K, Hansen B, Larsen KMH, Osterhus S, Johnson C, Jonsson S, Valdimarsson H (2021) Increased ocean heat transport into the Nordic Seas and Arctic Ocean over the period 1993-2016. Nat Clim Change 11(1):21–26

Vieira LEA, Solanki SK, Krivova NA, Usoskin I (2011) Evolution of the solar irradiance during the Holocene. Astron Astrophysics 531

Wang GL, Swanson KL, Tsonis AA (2009) The pacemaker of major climate shifts. Geophys Res Lett 36

Wang JL, Yang B, Fang M, Wang ZY, Liu JJ, Kang SY (2022) Synchronization of summer peak temperatures in the Medieval climate anomaly and Little Ice Age across the Northern Hemisphere varies with space and time scales. Clim Dyn 1–16. https://doi.org/10.1007/s00382-022-06524-6

Wu TW, Hu AX, Gao F, Zhang J, Meehl GA (2019) New insights into natural variability and anthropogenic forcing of global/regional climate evolution. NPJ Clim Atmos Sci 2(1):18

Wuebbles DJ, Fahey DW, Hibbard KA, Dokken DJ, Stewart BC, Maycock TK (eds) (2017) Climate Science Special Report: Fourth National Climate Assessment. Global Change Research Program, USGCRP Washington, DC, USA, U.S

Yao S-L, Huang G, Wu R-G, Qu X (2016) The global hiatus - a natural product of interactions of a secular warming trend and a multidecadal oscillation. Theor Appl Climatol 123:349–360

Yao SL, Luo JJ, Huang G, Wang PF (2017) Distinct global warming rates tied to multiple ocean surface temperature changes. Nat Clim Change 7(7):486–491